Hindawi
Shock and Vibration
Volume 2023, Article ID 5097144, 19 pages
https://doi.org/10.1155/2023/5097144

Research Article

Study on Fault Feature Extraction of Rolling Bearing Based on Improved WOA-FMD Algorithm

Guangfei Jia and Yanchao Meng

School of Mechanical Engineering, Hebei University of Science and Technology, Shijiazhuang 050018, China

Correspondence should be addressed to Guangfei Jia; jiagf_11@163.com

Received 20 April 2023; Revised 30 May 2023; Accepted 31 May 2023; Published 14 June 2023

Academic Editor: Xingxing Jiang

The vibration signal of rolling bearing fault is nonlinear and nonstationary under the interference of background noise, and it is difficult to extract fault features from it. When feature mode decomposition is used to analyze signals, prior parameter settings can easily affect the decomposition results. Therefore, a fault feature extraction method based on improved whale optimization algorithm is proposed to optimize feature modal decomposition parameters. The improved WOA integrates Lévy flight and adaptive weight, and envelope entropy is used as fitness function to optimize feature modal decomposition parameters. The feature mode decomposition of the original signal is performed using the optimal combination of parameters to obtain multiple IMF components. The optimal IMF component envelope demodulation analysis is selected according to the kurtosis value, and the fault feature is extracted through the envelope spectrum. Comparing the LMWOA method with PSO and WOA methods by simulated and experimental signals, the results show that the optimization speed of LMWOA is faster than that of other methods. Compared with CEEMD, VMD, and FMD methods, the improved WOA-FMD method has higher fault feature ratio and can accurately extract fault features under noise interference. This method can effectively solve the parameter adaptive ability and improve the accuracy of fault diagnosis, which has practical significance.

1. Introduction

As a standard component in industrial production field, bearing is widely applied in aerospace, energy, transportation, manufacturing, and other fields [1–3]. Because the bearings are used to support the rotating parts of machinery and bear various dynamic loads, they are prone to various faults during their operation [4, 5]. Therefore, it is necessary to monitor the running state of the bearing and diagnose the fault types in time. This is of great significance to the safe and reliable operation of mechanical equipment and the reduction of equipment loss.

In the process of collecting vibration signals, the complex working environment makes the vibration signal mixed with a lot of noise. The signal usually presents a nonlinear and nonstationary state [6]. In order to solve this problem, EMD, EWT, and VMD have been widely studied and applied in fault diagnosis [7–9].

Huang et al. [10] proposed a time signal decomposition method called EMD, which can adaptively decompose the signal into several intrinsic mode functions according to the characteristics of the data. Guo et al. [11] combined the shape controlling parameter based on cubic spline interpolation with EMD, and it has been applied to fault diagnosis of rolling bearing and achieved good results. However, the application effect of EMD in mechanical fault diagnosis is limited by mode overlap and boundary effect [12, 13]. Wu et al. [14] proposed EEMD, which decreases the effect of mode mixing by adding white noise, but it cannot effectively solve the problem of endpoint effect [15]. Yeh et al. [16] proposed that CEEMD can decompose such nonstationary signals very well. Although the decomposition ability has been improved, a large number of noise residues still exist in the signal.

Gilles [17] proposed EWT based on wavelet transform. EWT is generated by splitting the Fourier spectrum, and

binary band allocation may divide feature signals into different modes [18]. To solve the above problems, Dragomiretskiy and Zosso [19] proposed a VMD algorithm which can adaptively decompose through center frequency and bandwidth constraints. VMD essentially sets a set of Wiener filters, which adaptively decompose the signal into multiple narrowband signals with different frequencies. This avoids mode aliasing [20]. Jiang et al. [21] used the convergence trend phenomenon to quickly and adaptively determine the number of potential modes and the optimal initial center frequency of the signal. Based on this research, central frequency mode decomposition is proposed to better solve the problem of parameter adaptation [22]. Song et al. [23]overcame the problem of model parameter predefined in multivariate variational mode decomposition by using smart multichannel mode extraction and manifold learning methods.

Miao et al. [24] proposed a new decomposition mode—FMD, inspired by adaptive signal decomposition and deconvolution techniques. FMD is deduced from multiple FIR filter banks and calculating the maximum correlation peak deconvolution. It can consider the pulse property and periodicity of the signal at the same time and has good noise robustness. FMD algorithm requires manual input parameters, and different parameters have different effect on the final results, so it is not applicable. Yan et al. [25] proposed a PSO method to optimize the decomposition number of mode and filter length of FMD, which guarantees the parametric adaptability of feature mode decomposition. However, the influence of the number of frequency bands on the decomposition results is neglected, and the iteration of PSO is prone to premature phenomenon and falls into local optimal solution [26, 27]. Mirjalili and Lewis [28] proposed WOA to observe and simulate the predatory behavior of whales in 2016. WOA has the advantages of simple structure, fast searching speed, less parameters, and strong global convergence. In WOA, with the number of iterations increasing, the convergence speed of the algorithm gradually increases. It is easy to fall into a local optimal solution [29, 30].

Under the interference of background noise, the EMD, CEEMD, and VMD algorithms are difficult to extract the fault characteristics of rolling bearings. When the signal is decomposed by the FMD method, in addition to the number of decomposed modes and the length of the filter, the number of frequency bands will also affect the decomposition results. Therefore, the number of frequency bands should also be included in the parameter optimization. Although whale optimization algorithm has advantages over particle swarm optimization algorithm in optimization speed and accuracy, it is easy to fall into local optimization in the process of optimization. This leads to the failure to achieve the optimal decomposition effect. In order to overcome the above problems, this paper proposes an improved WOA-FMD algorithm. This method introduces adaptive weights and Lévy flight into WOA. The envelope entropy is used as the fitness function of the algorithm to optimize the FMD parameters. The kurtosis value is used as an index for Hilbert envelope demodulation analysis to extract the fault characteristic frequency of the signal.

2. Fundamental Algorithms

2.1. Feature Mode Decomposition. FMD is a new nonrecursive signal decomposition method, mainly including the steps of designing FIR filter bank, updating filter, calculating cycle, and calculating decomposition mode. By initializing the filter bank and iteratively updating its coefficients, different modes can be selected simultaneously and adaptively. Figure 1 displays the flowchart of FMD algorithm, and the algorithm is as follows:

(1) *Step 1*. Read the collected raw signal x and set FMD decomposition mode n, FIR filter bandwidth L, and iteration number I of FMD.

(2) *Step 2*. The FIR filter bank is initialized using K Hanning windows, and set start iteration $i = 1$.

(3) *Step 3*. Use $u_k^i = x * f_k^i$ to obtain a signal to remove interference, that is, the IMF components obtained after decomposition, where $k = 1, 2, ...K$, and $*$ represents the convolution operation.

(4) *Step 4*. The filter coefficients are periodically updated based on the initial input signal x, the number of decomposed modes u_k^i, and the estimated fault frequency T_k^i. T_k^i is the time delay when the autocorrelation spectrum R_k^i of u_k^i reaches a local maximum after the first zero crossing.

(5) *Step 5*. Determine whether the current number of iterations has reached the maximum number of iterations. If it is not satisfied, go back to step 3 and repeat the iteration. Otherwise, proceed to step 6.

(6) *Step 6*. Calculate the CC between two adjacent components and construct a correlation matrix with $CC_{(K\times K)}$. Select two adjacent modal components with the largest correlation coefficient and calculate their correlation kurtosis according to the estimated fault period . Finally, the modal component with large correlation kurtosis is selected as the modal component of FMD, set $K = K - 1$.

(7) *Step 7*. Determine if the specified n is the same as the number of modes K. If not, go back to step 3. Otherwise, the iteration stops and the modal component of the output FMD is n, which is the final decomposition result.

2.2. Whale Optimization Algorithm. The WOA algorithm mainly includes three kinds of predator-prey behavior simulation methods: surrounding prey, bubble net predator, and prey search. The specific steps are as follows:

(1) *Step 1*. When searching the prey position is unknown, the WOA assumes that the solution with the smallest fitness among individuals in the current population is the target or closest prey and updates the position of other search individuals after defining the optimal solution. When $p < 0.5$ and $|A| < 1$, the behavior of surrounding prey is executed, and the update formula is

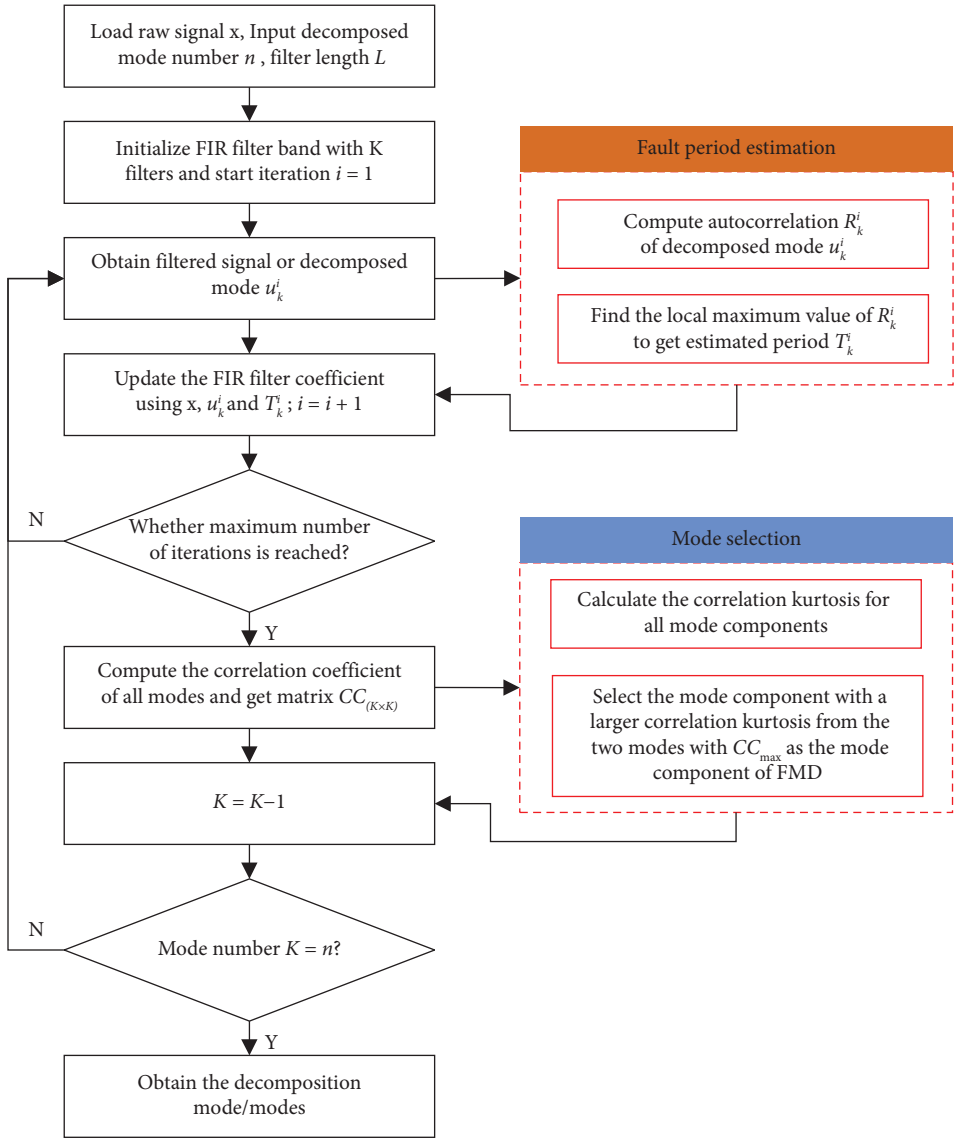

Figure 1: Flowchart of FMD.

$$\begin{cases} a = 2 - T \cdot \left(\dfrac{2}{T_{\max}}\right), \\ A = 2 \cdot a \cdot rand() - a, \\ C = 2 \cdot rand(), \\ D = \left|C \cdot X^*(t) - X(t)\right|, \\ X(t+1) = X^*(t) - A \cdot D, \end{cases} \tag{1}$$

where a linearly decreases to 0 in the iteration process; T is the current iteration number; and $T_{\max}$ is the maximum iteration number; A and C are synergy coefficients; $rand()$ is a random number generated from the $(0, 1)$ interval; D is the distance between the optimal whale and the current whale; $X^*(t)$ is the current optimal solution position; $X(t)$ is the current solution position; and $X(t+1)$ is the position of the whale after moving to the optimal solution position.

(2) *Step 2*. When $p \geq 0.5$, the precontraction behavior of the bucket net predation of whales is simulated, and the position update formula is

$$\begin{cases} X(t+1) = D \cdot e^{bl} \cdot \cos(2\pi l) + X^*(t), \\ D = \left|X^*(t) - X(t)\right|, \end{cases} \tag{2}$$

where b is a constant and assumes a spiral shape and L is a random number that oscillates at $[-1, 1]$.

(3) *Step 3*. When $p < 0.5$ and $|A| \geq 1$, WOA will enter the global search and randomly find the position of a search body in the population to replace the found optimal position. It no longer updates the position

according to the found optimal position, which enhances the search energy of the algorithm. The formula is

$$\begin{cases} a = 2 - T \cdot \left(\dfrac{2}{T_{\max}}\right), \\ A = 2 \cdot a \cdot rand() - a, \\ C = 2 \cdot rand(), \\ D = \left|C \cdot X_1(t) - X(t)\right|, \\ X(t+1) = X_1(t) - A \cdot D, \end{cases} \tag{3}$$

where X_1 is the random selection of the whale position.

(4) *Step 4*. When $T = T_{\max}$, max reaches the maximum number of iterations, and the convergence factor a linearly decreases to 0, the best search agent is output. If not, return to continue iteration.

3. Feature Extraction Based on Improved WOA

3.1. Improved WOA. WOA is simpler and more effective than other algorithms, but it is easy to fall into local optimum in the optimization process, resulting in a decrease in the accuracy of the results. The Lévy flight process adopts the search method of long-term small steps and occasional long-distance jumps, which helps WOA to expand the search scope and enhance the global exploration and search ability. This can prevent the solution from producing local optima and accelerate the convergence speed [31]. The formula for Lévy flight random step is calculated as follows:

$$levy: u = t^{-\lambda}, 1 \le \lambda \le 3. \tag{4}$$

Random numbers are solved using the Mantegna [32] method of normal fractions to generate a random step of the Lévy distribution, which is formulated as

$$s = \frac{\mu}{|v|^{1/\beta}}, \tag{5}$$

where β Is constant, and the value range is $0 < \beta < 2$. Take $\beta = 1.5$; $u \sim N(0, \sigma^2)$; $v \sim N(0, 1)$. The formula for calculating σ is given by

$$\sigma = \left\{\frac{\Gamma(1+\beta) \cdot \sin(\pi\beta/2)}{\beta\Gamma(1+\beta/2) \cdot 2^{(\beta-1)/2}}\right\}. \tag{6}$$

After introducing Lévy flight strategy, the position update formula of whale optimization algorithm is

$$X(t+1) = X(t) + \text{levy}(\lambda) \oplus A \cdot D. \tag{7}$$

In the WOA, the global search ability needs to be improved in the early stage, and the local search ability needs to be improved in the late stage. As the iteration time increases, the convergence speed of the algorithm increases. It will be prone to fail to jump out of the local optimal solution. In order to solve the problem, the inertia weight parameter, which can adjust the algorithm, is designed. The larger weight can be used for global optimization in a wide range, and the smaller weight can be used for local optimization near the optimal solution. The calculation principle of ω is

$$\omega = \cos\frac{\pi}{2} \times \left(1 - \frac{t}{T_{\text{MAX}}}\right), \tag{8}$$

where t is the current iteration number.

The improved whale optimization algorithm position update formula is

$$X(t+1) = \omega \cdot X(t) + \text{levy}(\lambda) \oplus A \cdot D. \tag{9}$$

In order to verify the performance of LMWOA, 10 basic standard test functions are used for experiments. The results are shown in Table 1 and Figure 2. Comparing the minimum value of the test function with the optimization results of the three algorithms, the optimization results of LMWOA are closer. According to Figure 2, it can be seen that the optimization speed of LMWOA is faster than that of the other two algorithms. After improvement, WOA can jump out of the local optimum faster, ensuring the accuracy of the algorithm.

3.2. Feature Extraction Process. The parameter decomposition mode n, filter length L, and frequency band number K in FMD have great influence on signal decomposition results. For example, if the filter length is too short, it may lead to poor filtering results. If the filter length is too long, it may lead to distortion and further increase the computational burden. If there are too many decomposed modes, the result may be redundant modes. The larger the number of bands is, the heavier the computational burden will be, which affects the decomposition performance to a certain extent.

Therefore, this paper uses LMWOA to optimize the parameters of FMD algorithm in order to get rid of the dependence of FMD on the prior knowledge of the fault cycle of the original signal and avoid the influence of human factors on the decomposition results. This can achieve the best decomposition effect. Its flowchart is shown in Figure 3. The LMWOA-FMD algorithm is implemented as follows:

(1) *Step 1*. Input the collected rolling bearing signal and put up (n, L, K) as the optimization parameters of the WOA. The optimization dimension is 4, the number of iterations $T_{\max} = 20$, and the number of search population is 15. In order to avoid under-decomposition or over-decomposition, the search space of decomposition mode number n is $[3, 7]$. In order to achieve a sample number that includes two adjacent repetitive transients related to bearing faults, the search space for the filter length L is assumed to be $[10, rand(f_s/f_g)]$, where $rand()$ is a rounding operation, and f_s and f_g are sampling frequency and bearing failure frequency,

Table 1: Results and comparison of different algorithms on 10 benchmark functions.

Function	Range	$f_{\min}$	PSO	WOA	LMWOA
$F_1(x) = \sum_{i=1}^{n} x_i^2$	$[-100, 100]$	0	$9.79e-4$	$1.10e-74$	$8.33e-290$
$F_2(x) = \sum_{i=1}^{n} \lvert x_i \rvert + \lim_{x \to \infty} \prod_{i=1}^{n} \lvert x_i \rvert$	$[-10, 10]$	0	0.020	$3.73e-51$	$1.31e-160$
$F_3(x) = \sum_{i=1}^{n} i x_i^2 + \text{random}(0, 1)$	$[-1.28, 1.28]$	0	0.163	$8.66e-4$	$1.21e-05$
$F_4(x) = -20\exp\left(-(1/5)\sqrt{1/n\sum_{i=1}^{n} x_i^2}\right)$ $-\exp\left(-(1/n)\sum_{i=1}^{n}\cos(2\pi x_i)\right) + 20 + e$	$[-32, 32]$	0	$5.66e-3$	$4.44e-15$	$8.88e-16$
$F_5(x) = (1/4000)\sum_{i=1}^{n} x_i^2 - \prod_{i=1}^{n} \cos(x_i/\sqrt{i}) + 1$	$[-600, 600]$	0	$1.84e-06$	0	0
$F_6(x) = (1/500 + \sum_{j=1}^{25}(j + \sum_{i=1}^{2}(x_i - a_{ij})^6)^{-1})^{-1}$	$[-65, 65]$	1	0.998	1	1
$F_7(x) = \sum_{i=1}^{11}[a_i - (x_1(b_i^2 + b_i x_2)/b_i^2 + b_i x_3 + x_4)]^2$	$[-5, 5]$	$3e-4$	$9.95e-4$	$3.57e-4$	$3.07e-4$
$F_8(x) = \frac{\pi}{n}\left\{10\sin(\pi y_1) + \sum_{i=1}^{n-1}(y_i - 1)^2 \times [1 + 10\sin^2(\pi y_{i+1})] + (y_n - 1)^2\right\}$ $+ \sum_{i=1}^{n} u(x_i, 10, 100, 4)$	$[-50, 50]$	0	0.103	0.023	0.016
$F_9(x) = [1 + (x_1 + x_2 + 1)^2(19 - 14x_1 + 3x_1^2 - 14x_2 + 6x_1x_2) + 3x_2^2]$ $[30 + (2x_1 - 3x_2)^2(18 - 32x_1 + 12x_1^2 + 48x_2 - 36x_1x_2 + 27x_2^2)]$	$[-2, 2]$	3	3	3	3
$F_{10}(x) = \sum_{i=1}^{4} c_i \exp(-\sum_{j=1}^{3} a_{ij}(x_j - p_{ij})^2)$	$[1, 3]$	-3.86	-3.862	-3.862	-3.859

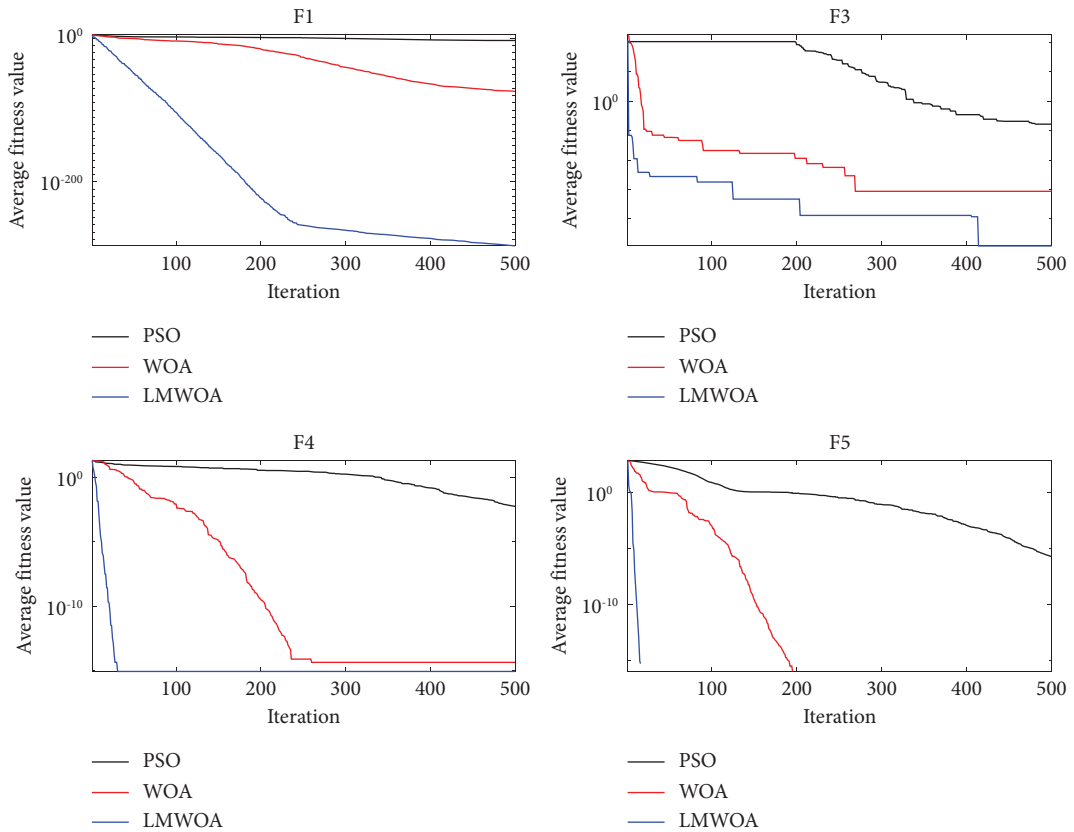

Figure 2: Convergence curve of the average fitness value of some selected functions.

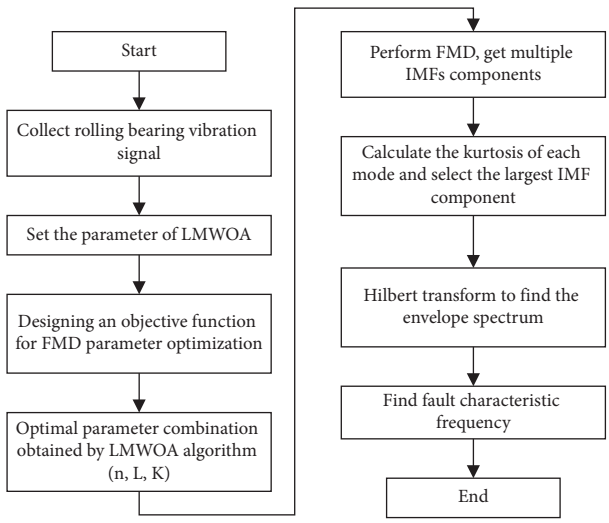

Figure 3: Flowchart of LMWOA-FMD algorithm.

respectively; K must be greater than n for the mode to decompose, so the search space of K is set as $[4, 10]$.

(2) *Step 2*. Set the envelope entropy as the judgment value of the fitness function. When the complexity of vibration signal is low and the noise interference is small, the envelope entropy is also small. On the contrary, when the feature information is small, the noise interference is larger and the envelope entropy is larger [33].

(3) *Step 3*. Obtain the optimal parameter combination (n, L, K) by using LMWOA to optimize the parameter combination.

(4) *Step 4*. Input the optimal parameter combination (n, L, K) into the FMD algorithm, disintegrate the signal into several IMF components, and use kurtosis value as the parameters of the target mode. Then, the kurtosis value of each component is calculated separately. When a bearing fault occurs, the vibration signal will deviate from the normal distribution under the action of fault impact, and the larger the kurtosis value, the richer the impact component and fault information.

(5) *Step 5*. Select the component with the highest kurtosis value as the target mode and calculate the envelope spectrum by Hilbert transformation to extract fault characteristics.

4. Case Study

4.1. Simulated Signal Analysis. The feasibility of the LMWOA-FMD method was verified by constructing the simulation signal of the inner ring fault of the rolling bearing, and the simulation signal expression is

$$\begin{cases} A_i = A_0 \cos\left(2\pi f_r t\right), \\ h(t) = e^{-ct} \sin\left(2\pi f_n t\right), \\ S(t) \sum_i A_i \left(t - iT - \tau_i\right), \end{cases} \tag{10}$$

where A_0 is the amplitude, $A_0 = 0.5$; f_r is frequency conversion, $f_r = 20Hz$; c is the attenuation factor, $c = 800$; f_n is the resonance frequency, $f_n = 4000Hz$; $S(t)$ is a periodic shock component; τ_i represents the small fluctuation of the ith shock with respect to period T; and fault frequency $f_i = 1/T$, $f_i = 120Hz$. In the simulation signal, $1dB$ Gaussian white noise interference is added, the sampling points are selected as 10240, and the sampling frequency $f_s = 12kHz$. The time-domain waveform diagram and sum spectrogram of the simulation signal after adding noise are shown in Figure 4.

The PSO, WOA, and LMWOA methods are, respectively, used to search the optimal parameter combination of FMD, and the minimum envelope entropy is used as the fitness function. The value change of fitness function is shown in Figure 5. In the figure, LMWOA-FMD converges to obtain the best solution when the number of iterations reaches 5 and final fitness function value is 9.08. Compared with PSO and WOA, LMWOA has better search ability, has faster convergence speed, and can seek the optimal FMD parameters faster. It is verified that Lévy flight and adaptive weights can effectively avoid falling into local optimum and improve algorithm performance, which can save a lot of time for optimization.

After optimization by LMWOA, the final optimal parameter combination is as follows: decomposition mode $n = 4$, filter length $L = 15$, and frequency band number $K = 5$. The parameters are input into FMD, and the decomposition effect is shown in Figure 6. The frequency of each mode component in the decomposition result is uniformly distributed, which avoids the appearance of mode aliasing and avoids losing some important information.

The kurtosis values of the four IMF components obtained after LMWOA-FMD treatment were calculated, respectively, and the results are shown in Table 2. After comparison of kurtosis values, IMF3 component is selected for Hilbert transform analysis of envelope demodulation, and its envelope spectrum is shown in Figure 7. According to the figure, it can be seen clearly that the extracted fault frequency is $120Hz$. At the same time, the dual frequency of $240Hz$ and the triple frequency of $360Hz$ are also accurately extracted. The inner ring failure frequency extracted by this method is near to the theoretical value, which means that the rolling bearing has inner ring damage. It is verified that this method can accurately identify fault characteristics under background noise and has certain noise robustness.

The FMD of prior parameters was compared, where decomposition mode number $n = 5$, filter length $L = 100$, and frequency band number $K = 6$. In Figure 8, there is no mode aliasing during FMD decomposition. However, most components have passband ripple, which has a certain impact on the final decomposition result.

At the same time, the CEEMD and VMD methods are also used to compare and verify. The number of mode decomposition of VMD is 5, and the penalty factor is 1500. The component with the maximum kurtosis value is continued to be used for envelope demodulation. The envelope spectra of the CEEMD, VMD, and FMD are shown in

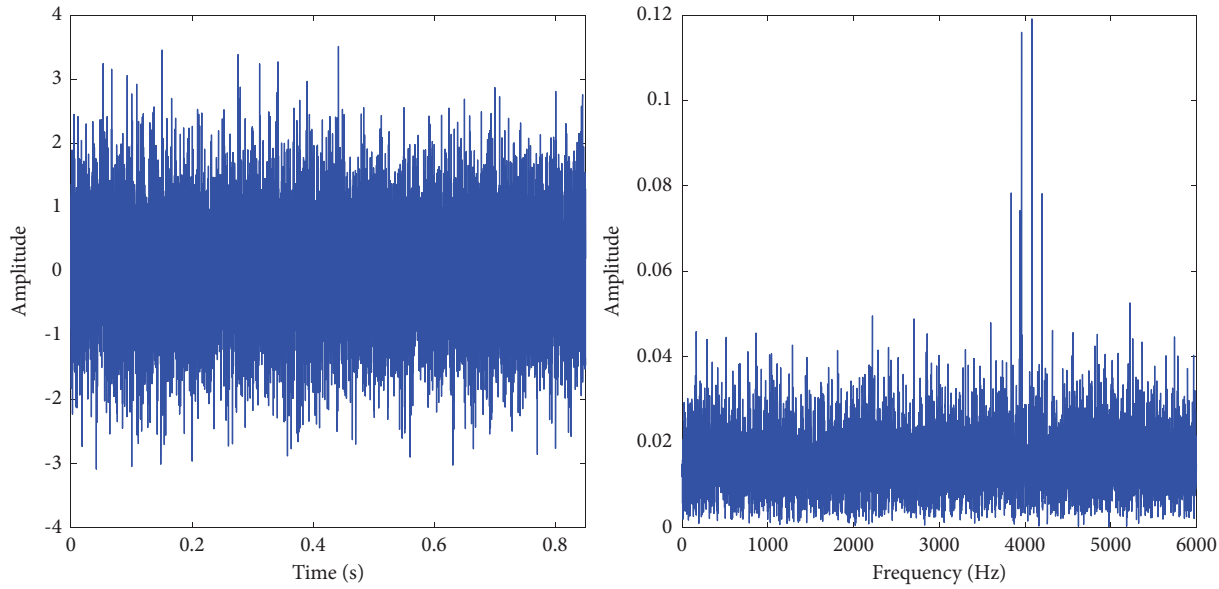

Figure 4: Time-domain waveform and spectrum of simulated inner ring fault signal.

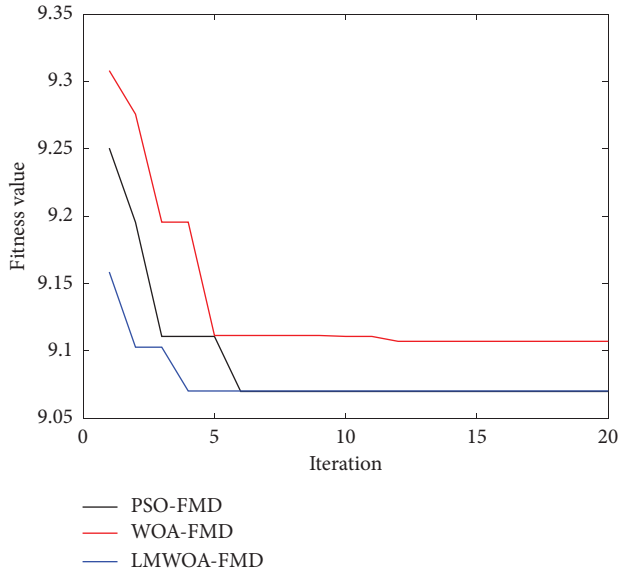

Figure 5: Fitness function value change of simulated inner ring fault signal.

Figure 9. In the figure, the envelope spectrum of CEEMD and FMD can extract the fault frequency under the interference of noise. However, there are many interference lines and the effect is not ideal. Further processing is required if the fault frequency is to be accurately extracted. The envelope spectrum of VMD method can accurately extract the fault frequency. However, the effect is not obvious due to the influence of the interference spectral line at the position of the second and third harmonic, and the robustness to noise is poor.

In order to further compare the advantages of these four methods, FFR is used as the evaluation index of the four methods. The larger the FFR value is, the more the periodic impact components are included in the IMF component [34]. The FFR is defined as

$$R_f = \frac{\sum_{k=1}^{m} S(kf)}{S}, \tag{11}$$

where S is the sum of the amplitude of the envelope spectrum; f is fault characteristic frequency; and $S(kf)$ is the amplitude of the envelope spectrum corresponding to each octave of the fault characteristic frequency.

Table 3 shows the FFR values corresponding to the four methods. The FFR value of LMWOA-FMD method is 0.059, which is higher than that of CEEMD, VMD, and FMD. This proves the superiority of this method.

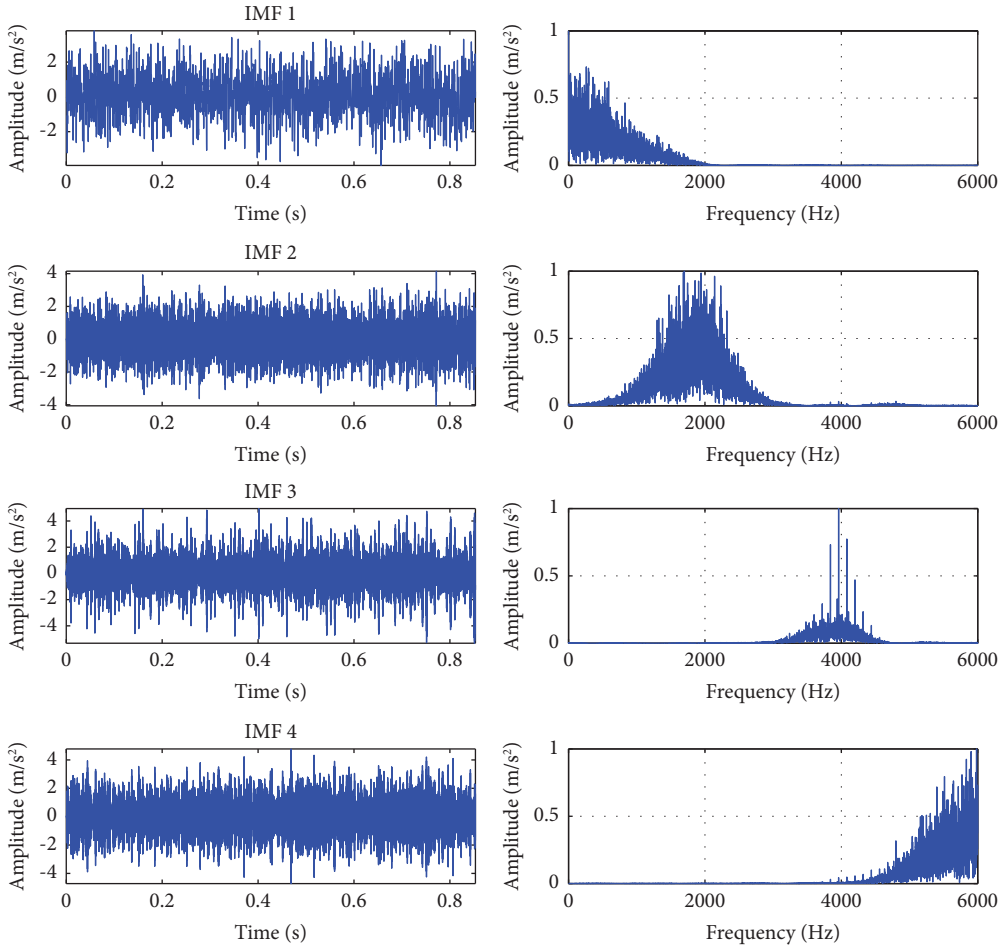

Figure 6: LMWOA-FMD result of simulated inner ring fault signal.

Table 2: Kurtosis value of each IMF component of simulated inner ring fault signal.

IMF	IMF1	IMF2	IMF3	IMF4
Kurtosis value	2.88	3	3.92	3.05

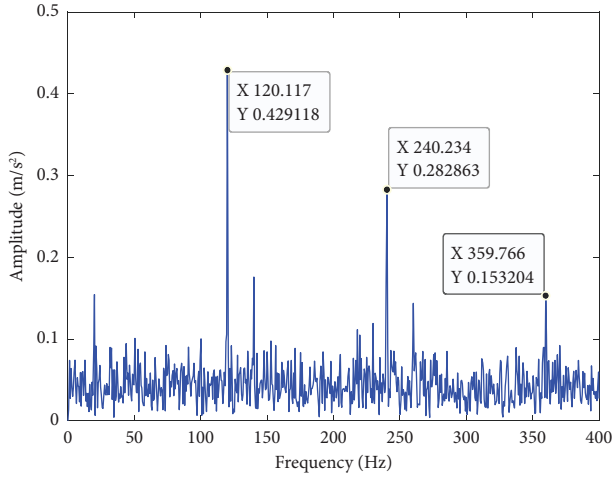

Figure 7: The analysis result by LMWOA-FMD method for the simulated inner ring fault signal.

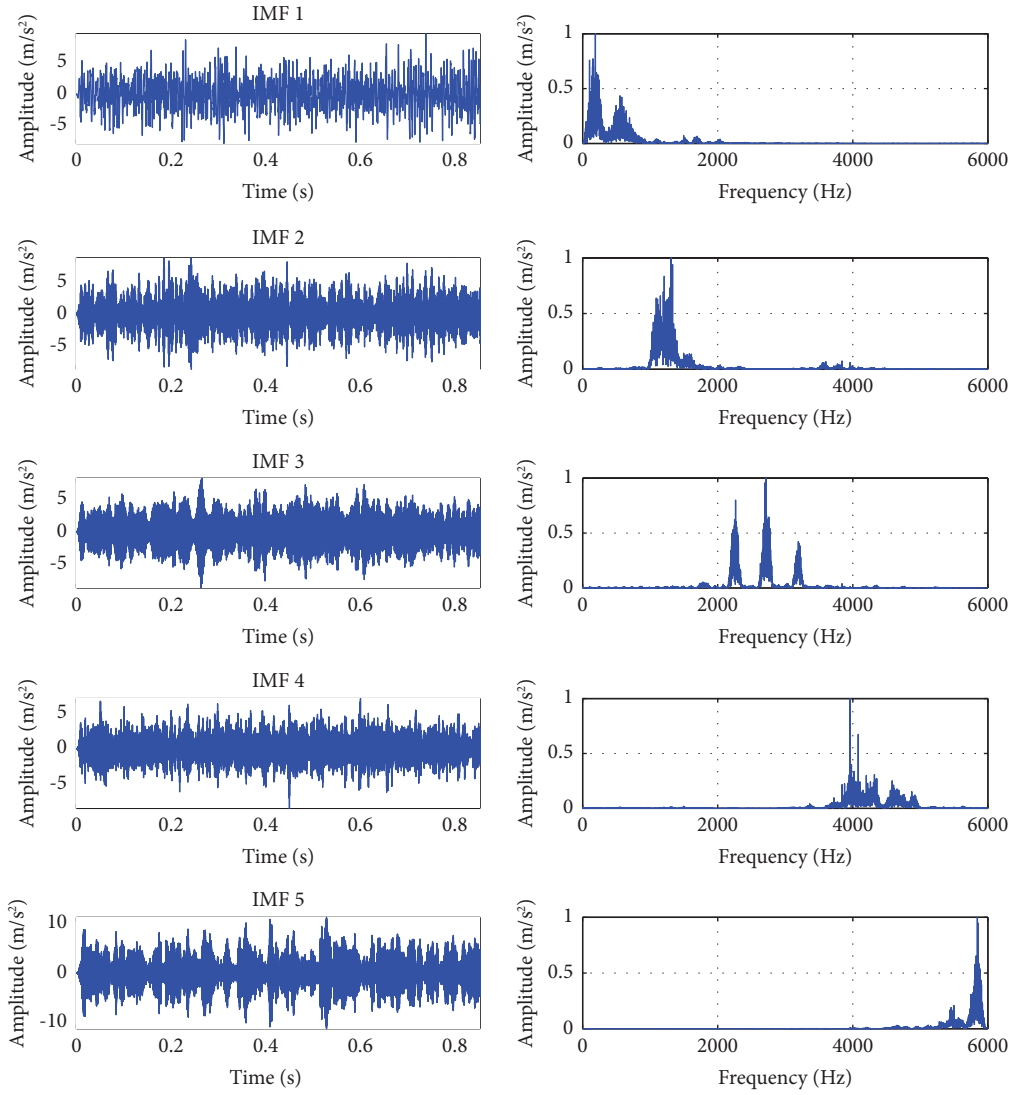

Figure 8: FMD result of simulated inner ring fault signal.

4.2. Experimental Signal Analysis. For the sake of further verifying the performance of the LMWOA-FMD method in practical application, the bearing dataset provided by CWRU [35] was used for experimental verification. The CWRU rolling bearing test stand is shown in Figure 10.

In the test bench, the driving end bearing of the induction motor with rated power of 1.5 kW and speed of 1797 r/min was selected as the research object. The bearing model was SKF6205-2RS deep groove ball bearing, and the sampling frequency was 12 kHz. The inner ring, outer ring, and roller components of the bearing were processed by the EDM method to produce tiny pits with the size of 0.117 mm to simulate the fault of the bearing. The bearing rotational frequency is 29.95 Hz, and the outer ring fault frequency is 107.3 Hz according to its parameters. The time-domain waveform and spectrum diagram with Gaussian white noise are shown in Figure 11.

The PSO, WOA, and LMWOA methods are, respectively, used to optimize FMD. The minimum envelope entropy is used as the fitness function to find the optimal parameter combination. The change of fitness function value is shown in Figure 12. The LMWOA-FMD in the figure converges to the optimal solution when the number of iterations reaches 3. The final fitness function value was 9.05. It is proved that the method avoids falling into local optimum and can accurately search the optimal solution. Compared with PSO and WOA, it has stronger searching ability, faster convergence speed, and faster searching for FMD optimal parameters.

The decomposition mode number $n = 4$, filter length $L = 34$, and frequency band number $K = 5$ are optimized by LMWOA. The parameters are input into FMD, and the decomposition effect is shown in Figure 13. The frequency belt of each modal component in the decomposition result is narrow, avoiding the phenomenon of mode overlap.

After carrying out LMWOA-FMD, four IMF components were obtained to calculate their kurtosis values, respectively, and the results are shown in Table 4. The component IMF3 with the largest kurtosis value is selected

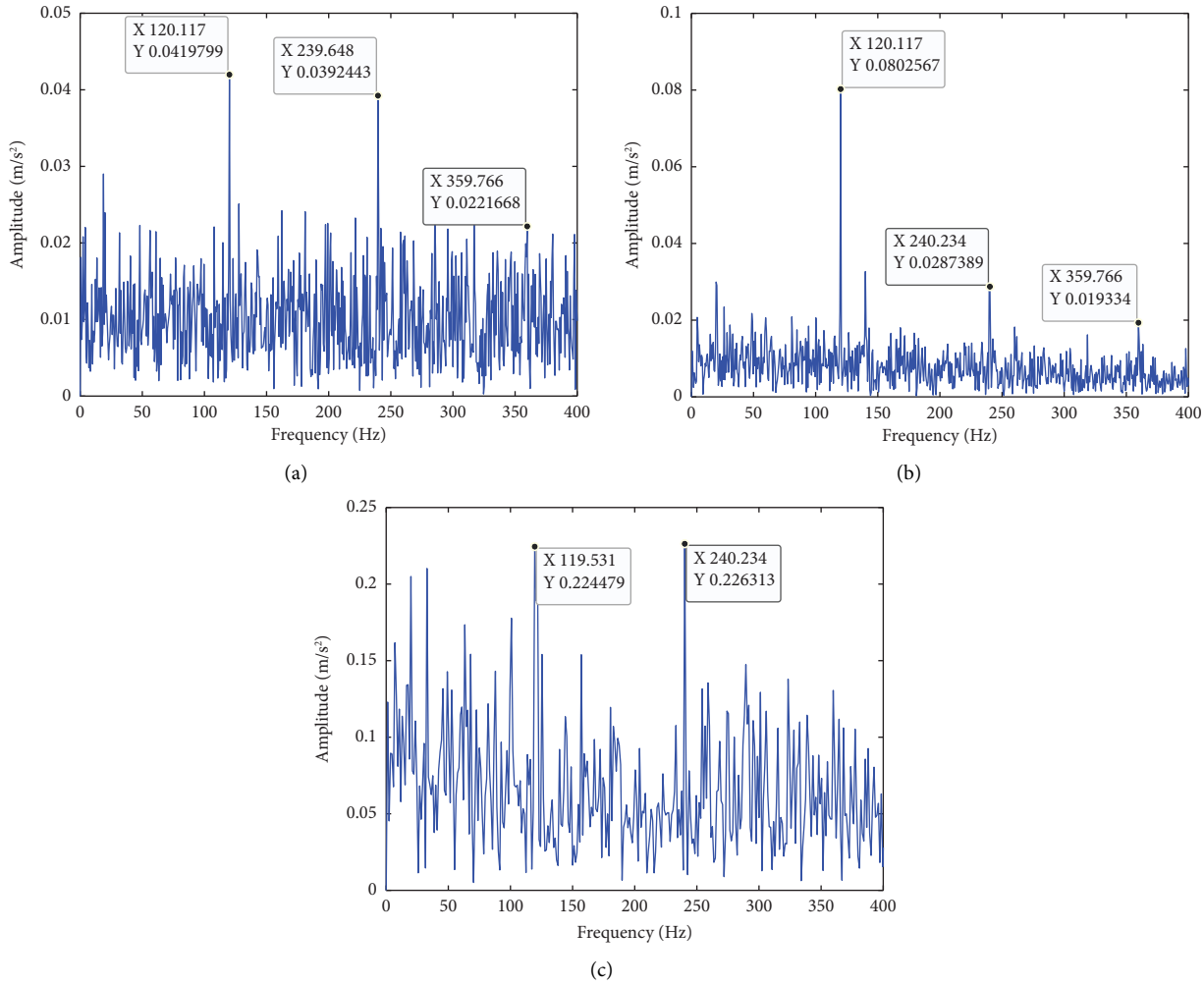

Figure 9: Analysis results of the simulated inner ring fault signal in different ways. (a) Result of CEEMD. (b) Result of VMD. (c) Result of FMD.

Table 3: The FFR of envelope spectra obtained by different methods for the analysis of simulated inner ring fault signal.

Method	LMWOA-FMD	FMD	VMD	CEEMD
FFR	0.059	0.024	0.043	0.025

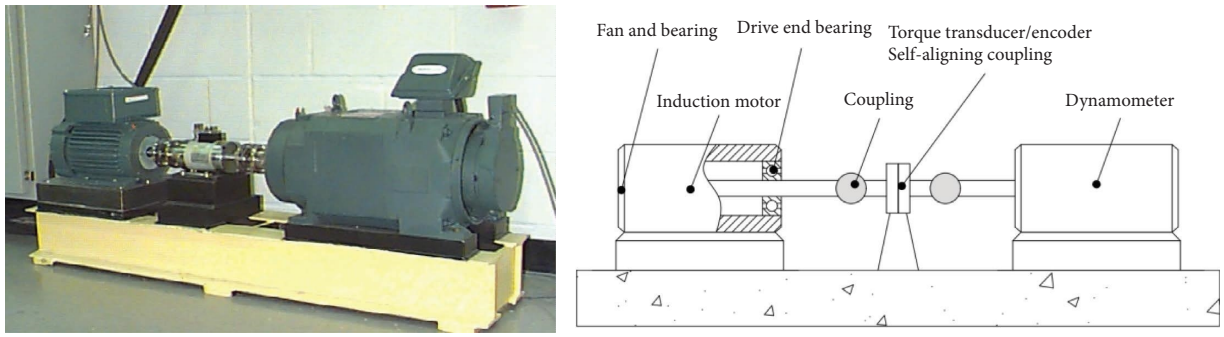

Figure 10: Rolling bearing fault simulation experimental device.

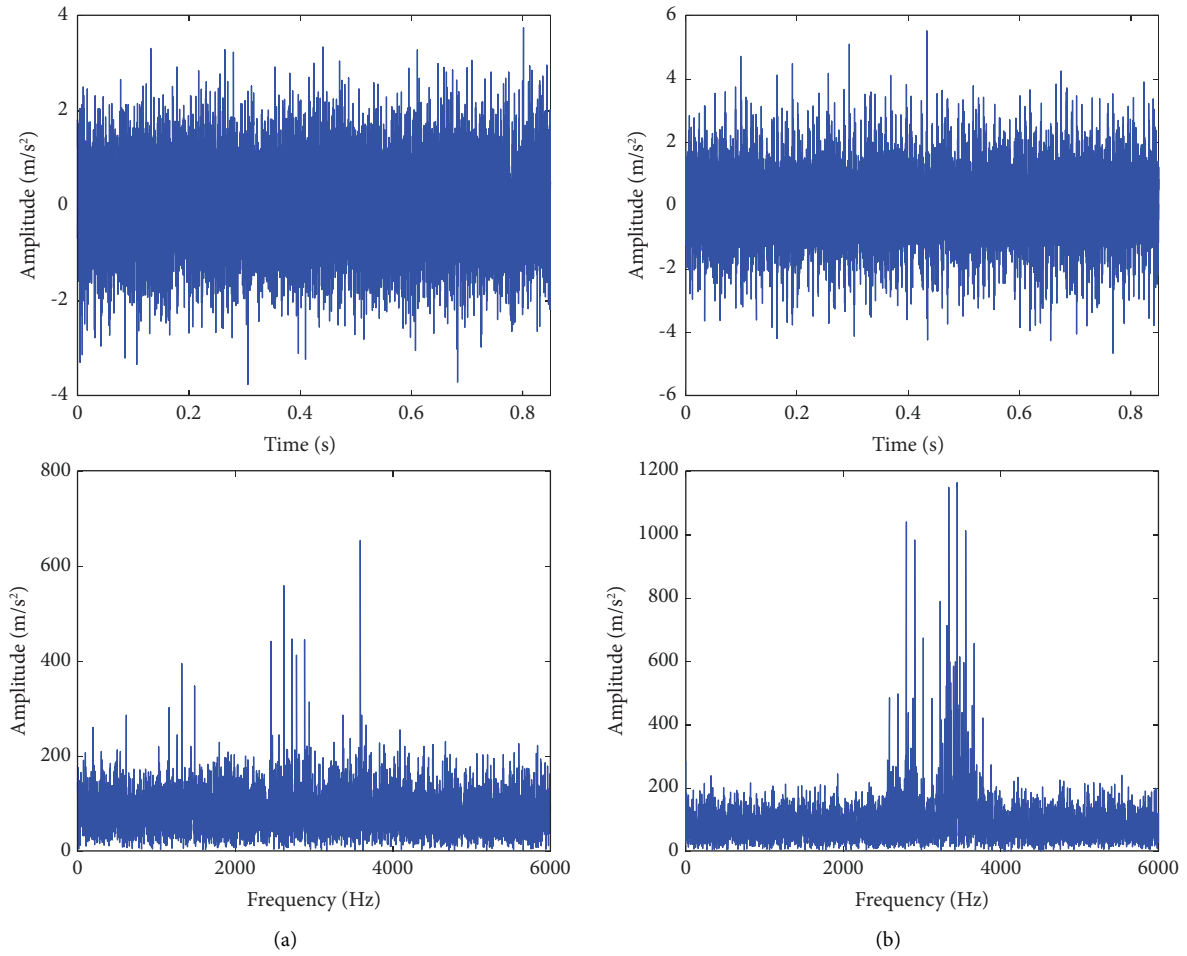

Figure 11: Time-domain waveform and spectra of experimental signals. (a) Inner race fault bearing vibration signal. (b) Outer race fault bearing vibration signal.

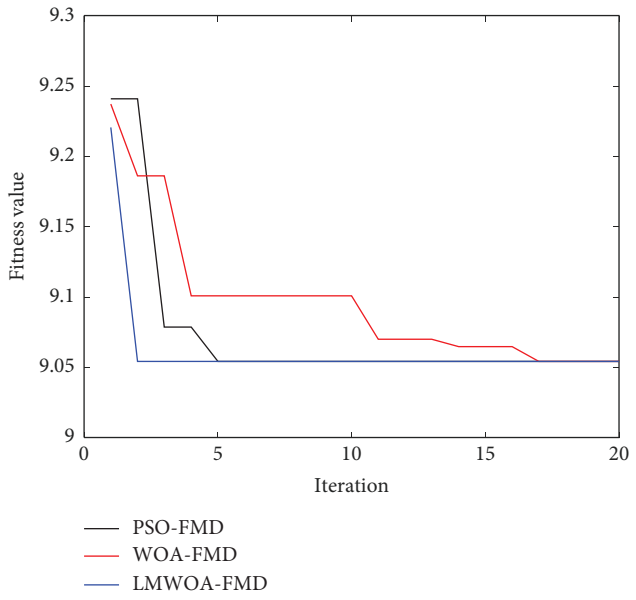

Figure 12: Fitness function value change of experimental outer ring fault signal.

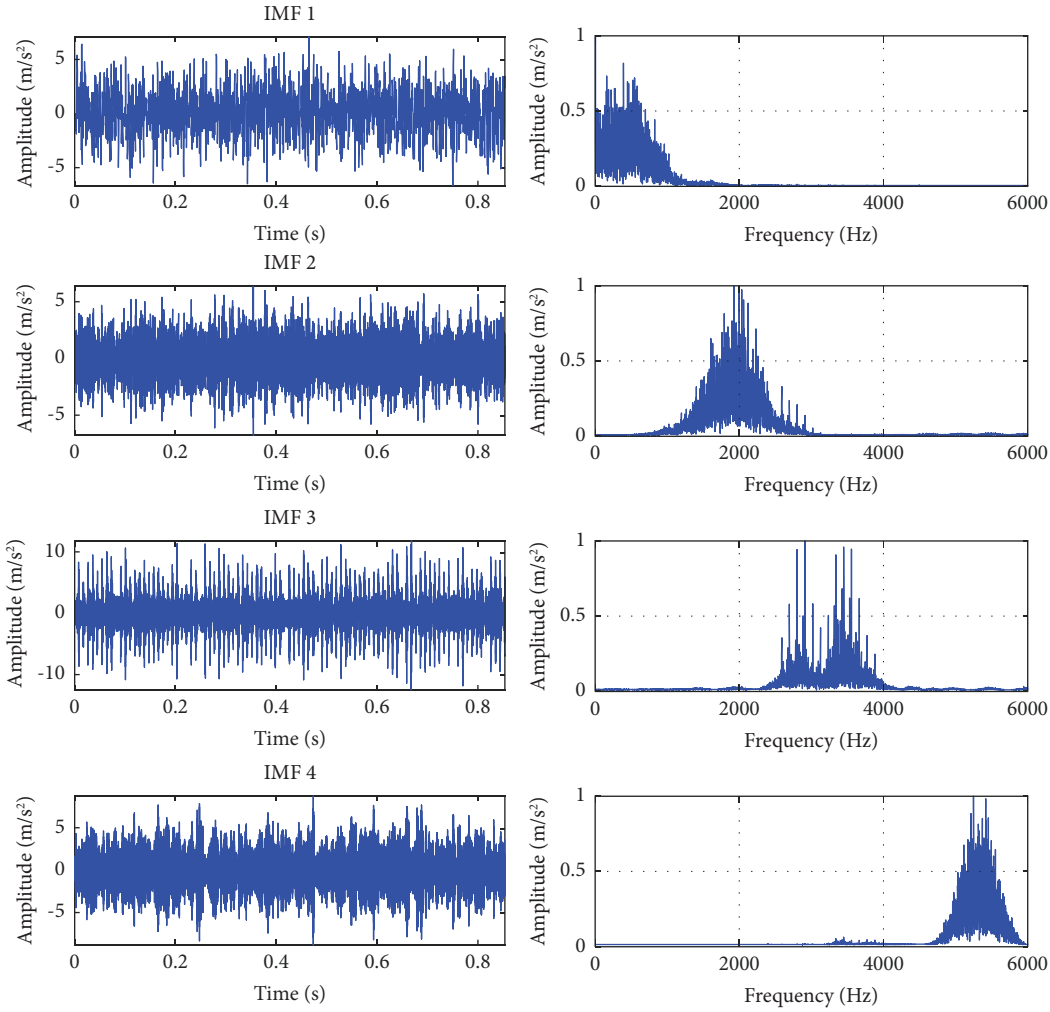

Figure 13: LMWOA-FMD decomposition result of experimental outer ring fault signal.

Table 4: Kurtosis values of IMF components of experimental outer ring fault signal.

IMF	IMF1	IMF2	IMF3	IMF4
Kurtosis value	3.516	3.119	6.182	3.049

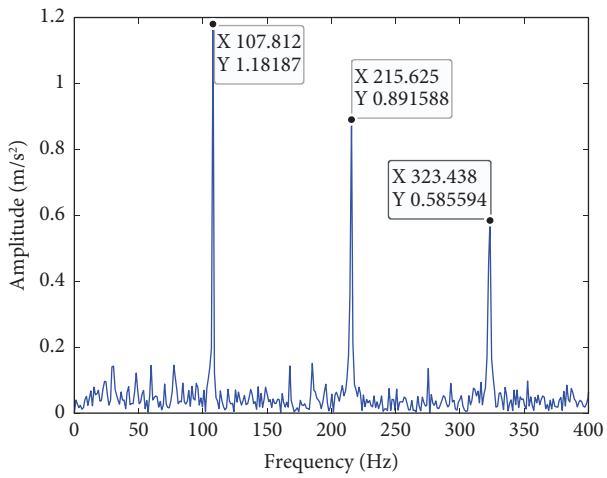

Figure 14: The analysis result by LMWOA-FMD method for experimental outer ring fault signal.

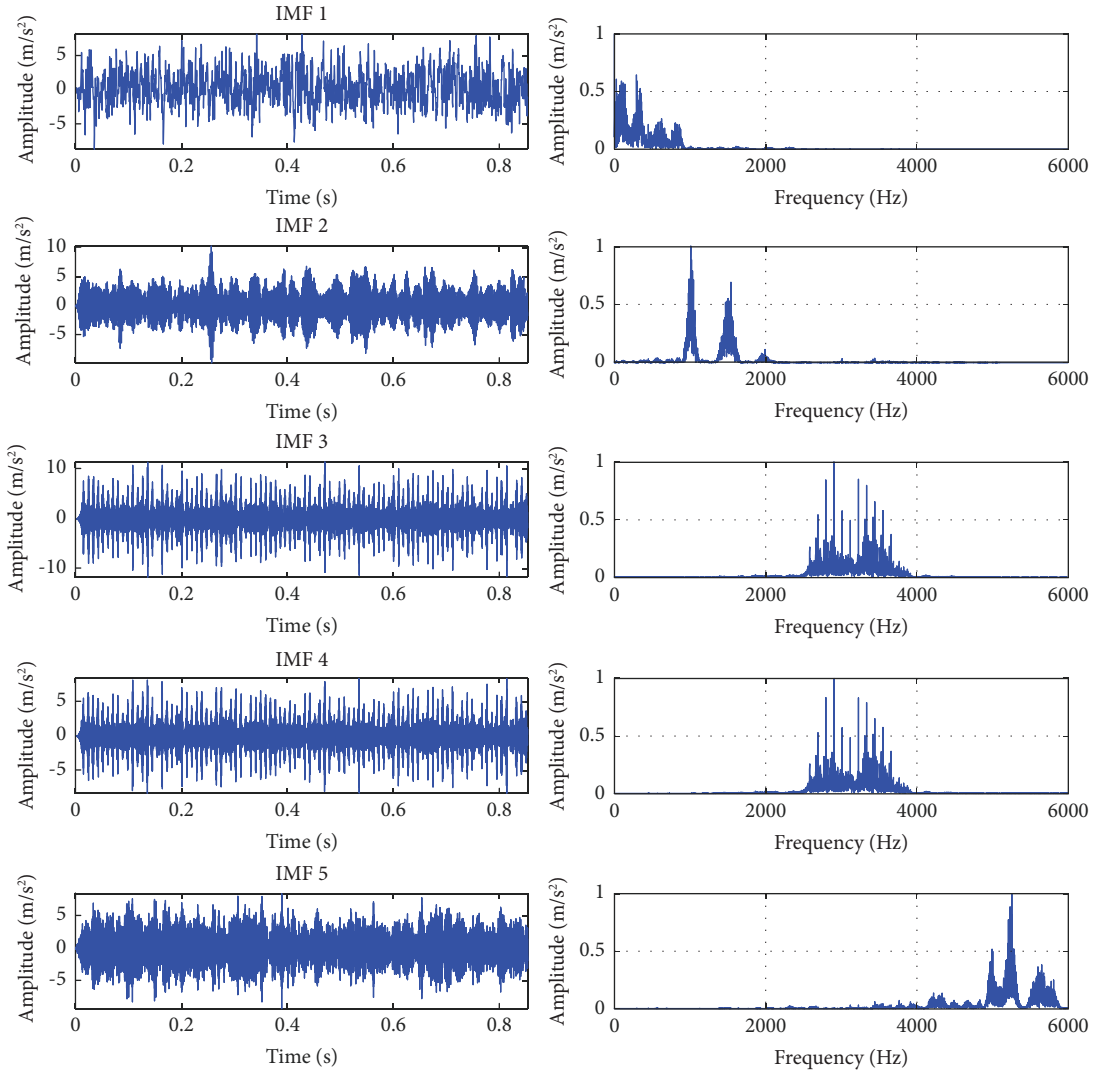

Figure 15: The analysis result by FMD method for experimental outer ring fault signal.

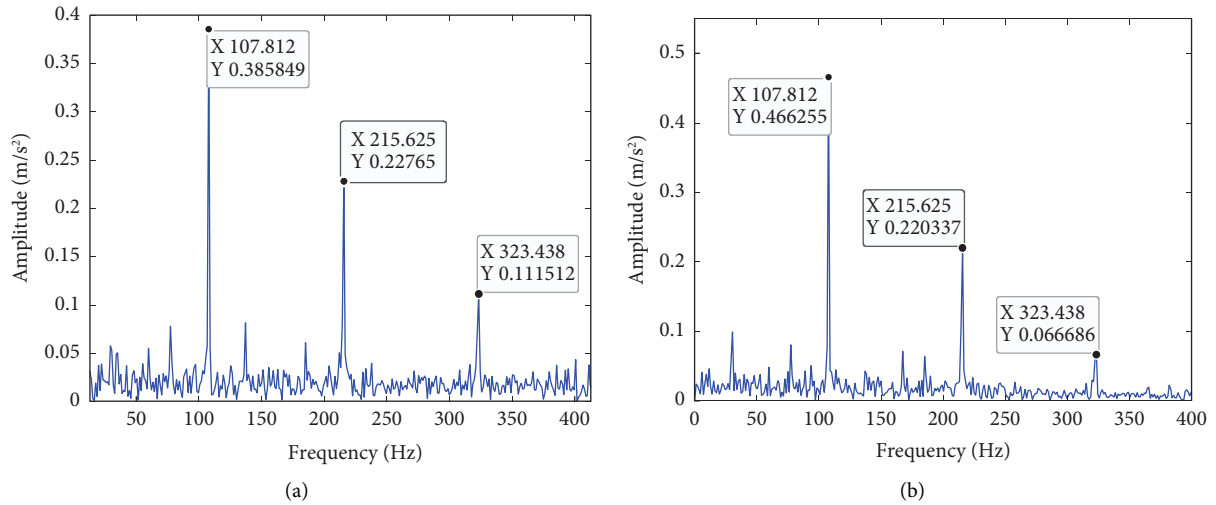

Figure 16: Continued.

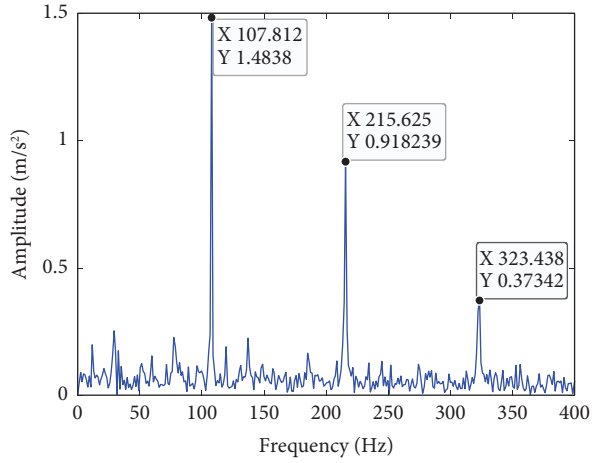

(c)

Figure 16: Analysis results of experimental outer ring fault signal in different ways. (a) Result of CEEMD. (b) Result of VMD. (c) Result of FMD.

Table 5: The FFR of envelope spectra obtained by different methods for the analysis of outer ring fault signal.

Method	LMWOA-FMD	FMD	VMD	CEEMD
FFR	0.122	0.096	0.106	0.084

to perform Hilbert transform for envelope demodulation analysis, and its envelope spectrum is shown in Figure 14. It can be clearly seen in the figure that the extracted fault frequency is $107.8Hz$, which is close to the theoretical value of $107.3Hz$. The frequency doubling characteristics can be clearly seen in the figure, and the spectral lines evenly distributed on both sides of the frequency doubling are low. It can be seen that this method can accurately extract the fault frequency under the noise while suppressing the influence of frequency conversion signal and noise on the fault signal and has certain robustness to noise.

The FMD of prior parameters was compared, where decomposition mode number $n = 5$, filter length $L = 100$, and frequency band number $K = 6$. The result is shown in Figure 15. In the figure, IMF2 and IMF5 have passband ripple and IMF3 and IMF4 have mode mixing. The signal is not well decomposed, and redundant information appears.

Furthermore, CEEMD and VMD methods are used to compare and verify the advantages of this method. The number of mode decomposition of VMD is 5, and the penalty factor is 1500. The envelope spectra of the CEEMD, VMD, and FMD are shown in Figure 16. In the figure, the envelope spectra of the three methods accurately extract the fault frequency. However, the amplitude effects of the second and third harmonic of the envelope spectrum are not significant. Compared with LMWOA-FMD, the overall extraction performance of the three methods is not ideal.

In order to further compare the advantages of these four methods, FFR is used as the evaluation index of the four methods. Table 5 shows the FFR values corresponding to other three methods. Among the four methods, the FFR value of the LMWOA-FMD algorithm is 0.122, which is greater than that of other three methods. It has been proven that this method has better noise resistance than other three methods.

The LMWOA-FMD method is used to decompose the inner ring signal of rolling bearing with Gaussian white noise. The optimized decomposition results are the number of decomposition modes $n = 4$, the filter length $L = 20$, and the number of frequency bands $K = 7$. The parameters are input into the FMD, and the decomposition result is shown in Figure 17. LMWOA-FMD divides the signal into four parts, avoiding redundant information and mode aliasing and avoiding the loss of important information.

After carrying out LMWOA-FMD, four IMF components were obtained to calculate their kurtosis values, respectively, and the results are shown in Table 6. The component IMF3 with the largest kurtosis value is selected to perform Hilbert transform for envelope demodulation analysis, and its envelope spectrum is shown in Figure 18. Although the spectrum line is cluttered under the influence of noise in the figure, the extracted fault frequency is prominent in the envelope spectrum, which is only $0.5Hz$ different from the theoretical value of $162.2Hz$, and twice the frequency of the fault feature can be extracted. It can be seen that the method can accurately extract the fault frequency under noise and has certain noise robustness.

After the same FMD parameters are imputed manually, the results are as shown in Figure 19. Passband ripple occurs in IMF2 and IMF5 components, which may cause a large amount of interference information in the signal after

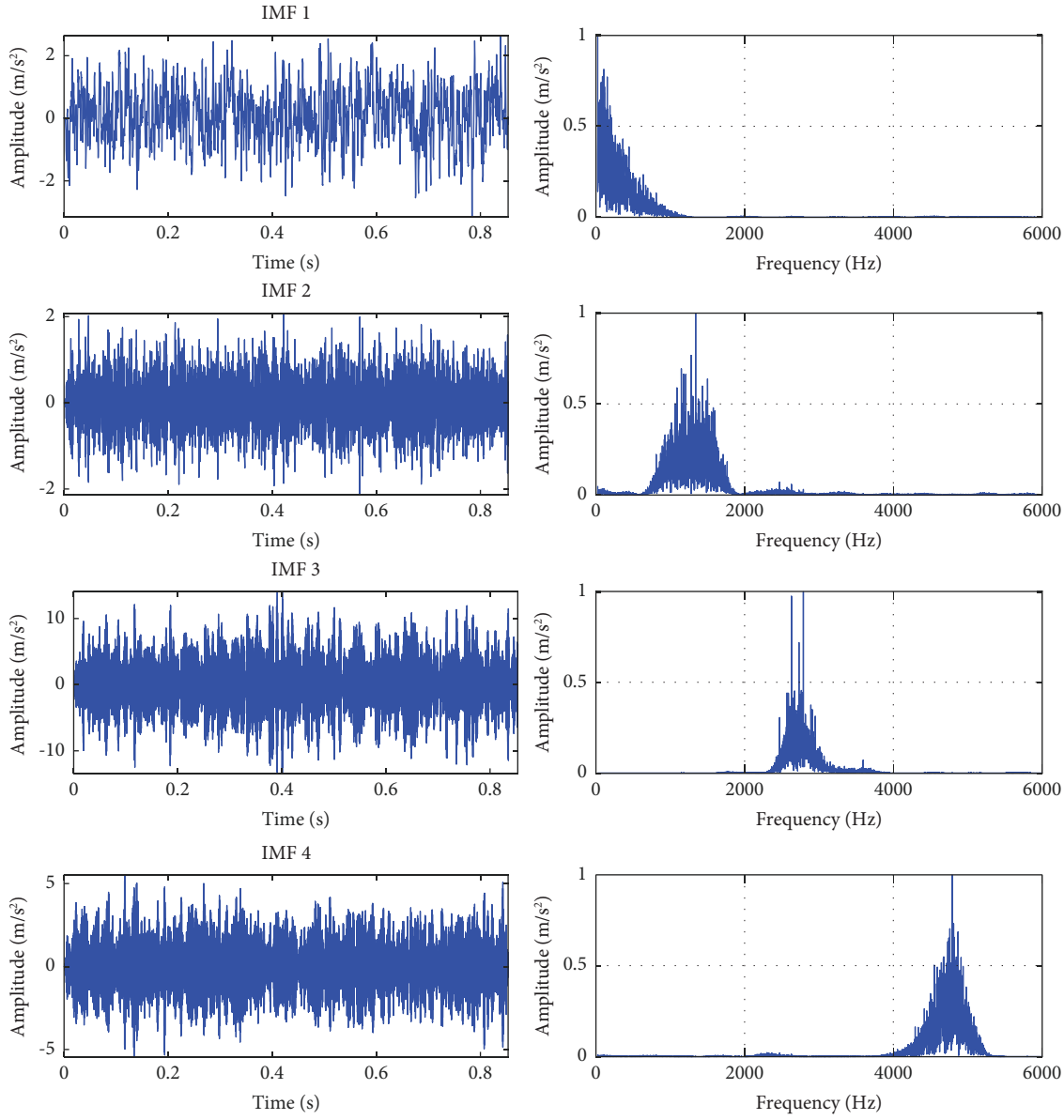

Figure 17: LMWOA-FMD decomposition result of experimental inner ring fault signal.

Table 6: Kurtosis value of each IMF component of experimental inner ring fault signal.

IMF	IMF1	IMF2	IMF3	IMF4
Kurtosis value	2.911	3.177	3.22	3.018

decomposition. This will affect the final result of fault feature extraction.

Also, input the signal to CEEMD and VMD, where the number of mode decomposition of VMD is 5 and the penalty factor is 1500. The envelope spectra of the three methods are shown in Figure 20. The fault frequencies of the envelope spectra of three methods in the figure are completely submerged by noise frequency and there are many interference lines, which make it impossible to extract fault features accurately. Compared with LMWOA-FMD, the two methods have poor noise resistance and cannot be applied in bearing fault diagnosis under noise background.

Table 7 shows the FFR values of four different methods. Among the four methods, the FFR value of the LMWOA-FMD algorithm is 0.022, which is greater than that of other three methods. It has been proven that the LMWOA-FMD method has better noise resistance than other three methods.

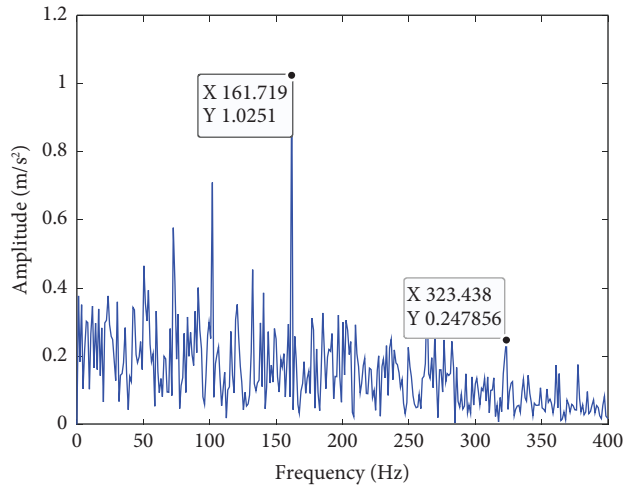

Figure 18: The analysis result by LMWOA-FMD method for experimental inner ring fault signal.

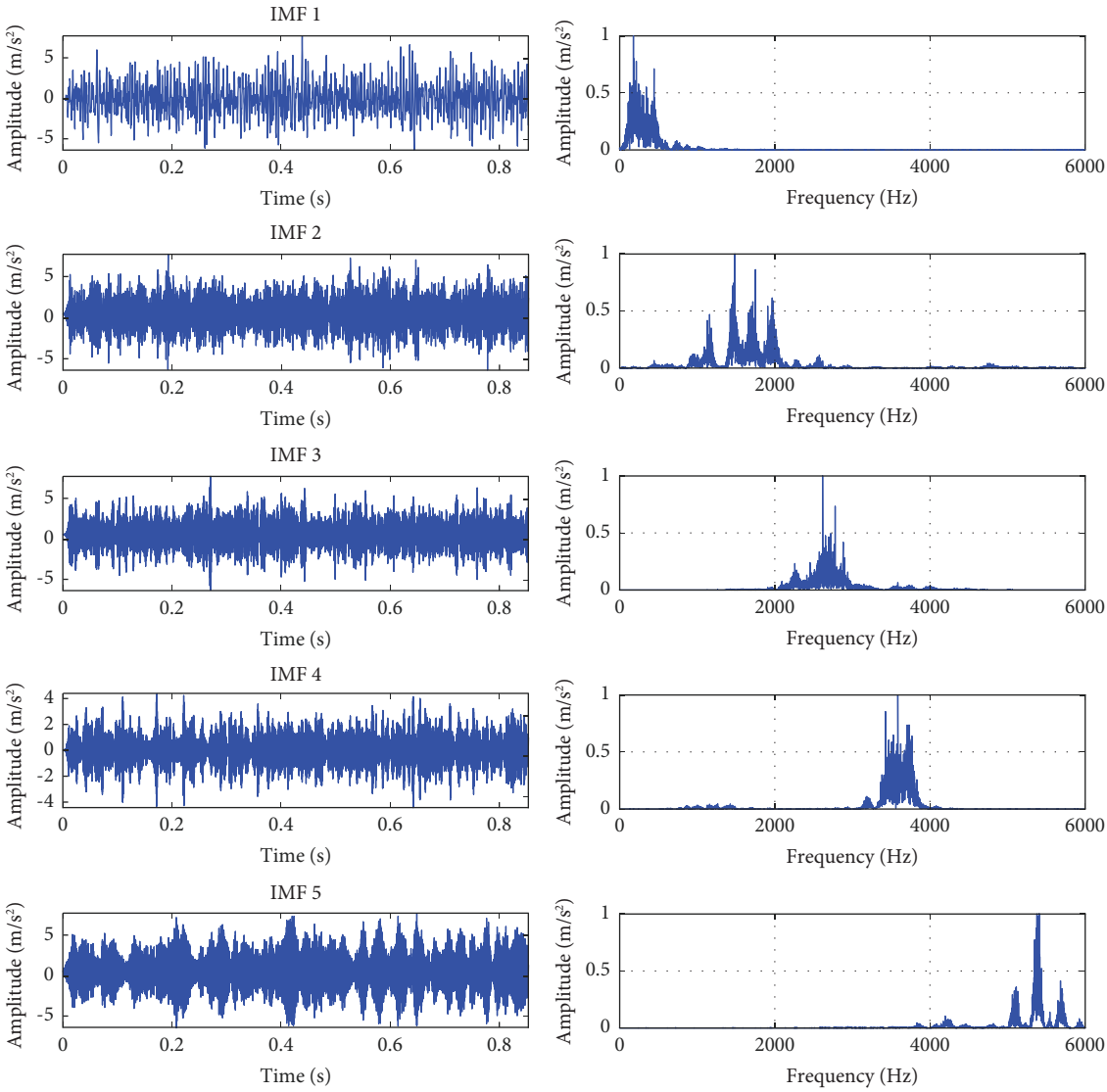

Figure 19: FMD decomposition result of experimental inner ring fault signal.

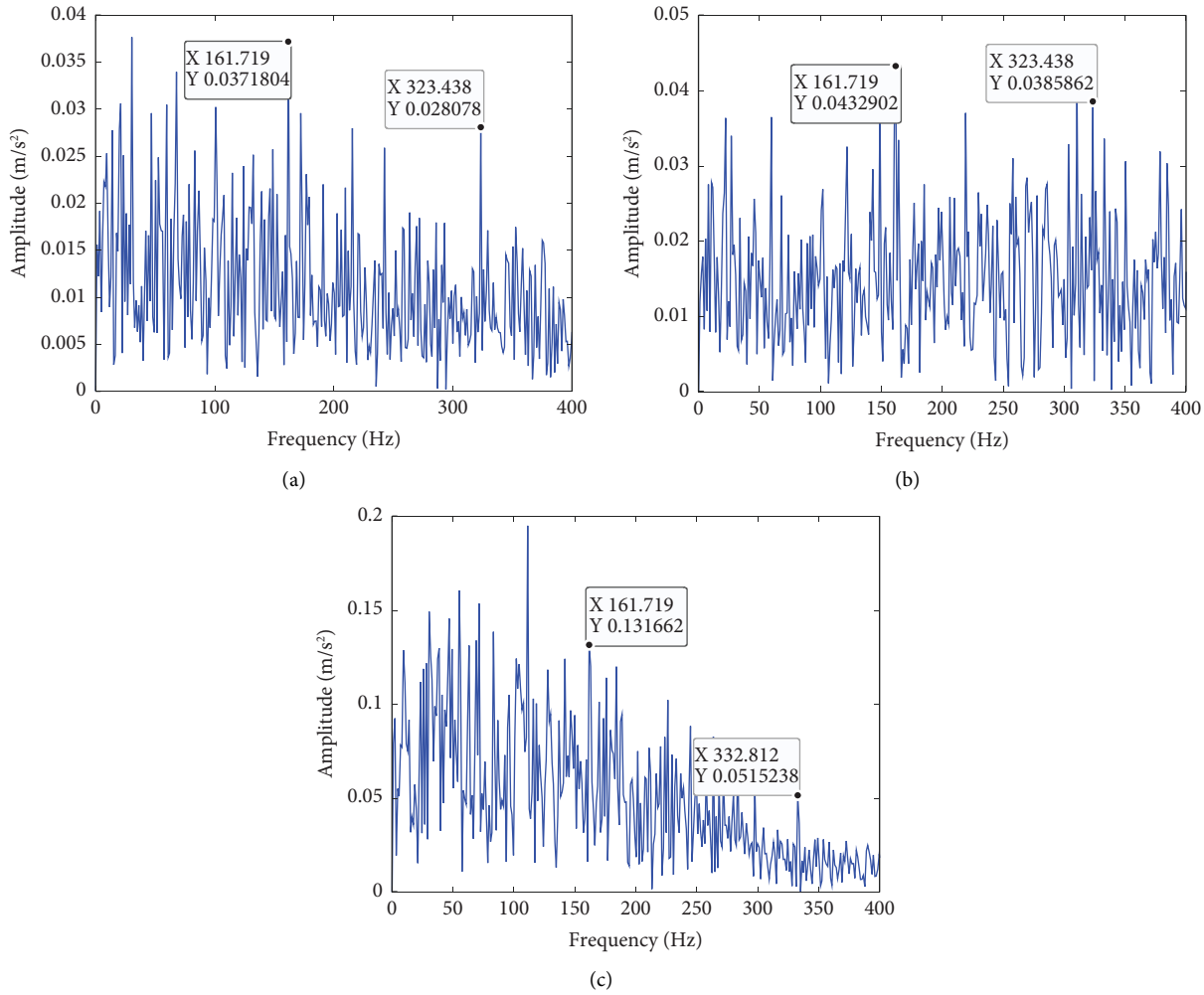

Figure 20: Analysis results of experimental inner ring fault signal in different ways. (a) Result of CEEMD. (b) Result of VMD. (c) Result of FMD.

Table 7: The FFR of envelope spectra obtained by different methods for the analysis of experimental inner ring fault signal.

Method	LMWOA-FMD	FMD	VMD	CEEMD
FFR	0.022	0.016	0.015	0.013

5. Conclusion

The improved WOA-FMD algorithm is proposed for fault feature extraction of rolling bearing under noise in this paper. The main contributions of the paper are as follows:

(1) The improved WOA with Lévy flight and adaptive weight can find the optimal value faster and more accurately than PSO and WOA in the optimization process of test function. It can find the optimal solution before 5 iterations in FMD optimization, which has stronger search ability and avoids falling into local optimal solution.

(2) The LMWOA-FMD algorithm successfully decomposes the original signal into multiple IMF components without mode aliasing and passband ripple. This overcomes the problem of input parameters by prior values and may realize the parameter adaptation of FMD. It can extract fault features better and improve the accuracy of signal decomposition.

(3) Through the analysis of simulated and experimental signals, the fault feature ratio extracted by this method in the background noise reaches 0.059 and 0.122. This is larger than the fault feature ratio of CEEMD, VMD, and FMD methods. It is proved that this method has strong noise robustness and can extract fault features more accurately.

Abbreviations

LMWOA: Lévy flight-based modified whale optimization algorithm
FMD: Feature mode decomposition
IMF: Intrinsic mode function
EMD: Empirical mode decomposition
EWT: Empirical wavelet transform
VMD: Variational mode decomposition

EEMD: Ensemble empirical mode decomposition
CEEMD: Complementary ensemble empirical mode decomposition
WOA: Whale optimization algorithm
FIR: Finite-impulse response
CC: Correlation coefficient
PSO: Particle swarm optimization
FFR: Fault feature ratio
CWRU: Case Western Reserve University
EDM: Electric discharge machining.

Data Availability

The data used to support the findings of this study are included within the article.

Conflicts of Interest

The authors declare that they have no conflicts of interest.

Acknowledgments

This research was supported by the Natural Science Foundation of Hebei Province (no. E2021208004).

References

[1] X. Zhang, Q. Miao, Z. W. Liu, Z. He, and J. He, "An adaptive stochastic resonance method based on grey wolf optimizer algorithm and its application to machinery fault diagnosis," *ISA Transactions*, vol. 71, pp. 206–214, 2017.

[2] T. Lin, G. Chen, W. Ouyang, Q. Zhang, H. Wang, and L. Chen, "Hyper-spherical distance discrimination: Hyper-spherical distance discrimination: A novel data description method for aero-engine rolling bearing fault detection novel data description method for aero-engine rolling bearing fault detection," *Mechanical Systems and Signal Processing*, vol. 109, pp. 330–351, 2018.

[3] Z. Jin, D. He, Z. Wei, D. Q. He, and Z. X. Wei, "Intelligent fault diagnosis of train axle box bearing based on parameter optimization VMD and improved DBN," *Engineering Applications of Artificial Intelligence*, vol. 110, Article ID 104713, 2022.

[4] Y. Kong, Z. Qin, Q. Han et al., "Enhanced dictionary learning based sparse classification approach with applications to planetary bearing fault diagnosis," *Applied Acoustics*, vol. 196, Article ID 108870, 2022.

[5] J. Gu, Y. X. Peng, H. Lu, X. D. Chang, and G. A. Chen, "A novel fault diagnosis method of rotating machinery via VMD, CWT and improved CNN," *Measurement*, vol. 200, Article ID 111635, 2022.

[6] W. G. Chen, J. N. Li, Q. Wang, and K. Han, "Fault feature extraction and diagnosis of rolling bearings based on wavelet thresholding denoising with CEEMDAN energy entropy and PSO-LSSVM," *Measurement*, vol. 172, Article ID 108901, 2021.

[7] Q. Gao, C. Duan, H. Fan, and Q. Meng, "Rotating machine fault diagnosis using empirical mode decomposition," *Mechanical Systems and Signal Processing*, vol. 22, no. 5, pp. 1072–1081, 2008.

[8] K. Yu, T. R. Lin, J. Tan, H. Ma, J. W. Tan, and H. Ma, "An adaptive sensitive frequency band selection method for empirical wavelet transform and its application in bearing fault diagnosis," *Measurement*, vol. 134, pp. 375–384, 2019.

[9] Z. Jin, D. He, R. Ma et al., "Fault diagnosis of train rotating parts based on multi-objective VMD optimization and ensemble learning," *Digital Signal Processing*, vol. 121, Article ID 103312, 2022.

[10] N. Huang, Z. Shen, S. Long et al., "The empirical mode decomposition and the Hilbert spectrum for nonlinear and non-stationary time series analysis," *Proceedings of the Royal Society of London. Series A: Mathematical, Physical and Engineering Sciences*, vol. 454, no. 1971, pp. 903–995, 1998.

[11] T. Guo, Z. Deng, and M. Deng, "An improved EMD method based on the multi-objective optimization and its application to fault feature extraction of rolling bearing," *Applied Acoustics*, vol. 127, pp. 46–62, 2017.

[12] H. Li, Y. Hu, F. Li, G. Meng, F. C. Li, and G. Meng, "Succinct and fast empirical mode decomposition," *Mechanical Systems and Signal Processing*, vol. 85, pp. 879–895, 2017.

[13] K. Zhang, Y. Xu, and P. G. Chen, Xu and P. Chen, Feature extraction by enhanced analytical mode decomposition based on order statistics filter," *Measurement*, vol. 173, Article ID 108620, 2021.

[14] Z. Wu, N. Huang, and E. E. Huang, "Ensemble empirical mode decomposition: a noise-assisted data analysis method," *Advances in Adaptive Data Analysis*, vol. 01, no. 01, pp. 1–41, 2009.

[15] L. Yu, W. Dai, and L. Tang, "A novel decomposition ensemble model with extended extreme learning machine for crude oil price forecasting," *Engineering Applications of Artificial Intelligence*, vol. 47, pp. 110–121, 2016.

[16] J. R. Yeh, J. S. Shieh, N. E. Huang, J. S. Shieh, and N. E. Huang, "Complementary ensemble empirical mode decomposition: a novel noise enhanced data analysis method," *Advances in Adaptive Data Analysis*, vol. 02, no. 02, pp. 135–156, 2010.

[17] J. Gilles, "Empirical wavelet transform," *IEEE Transactions on Signal Processing*, vol. 61, no. 16, pp. 3999–4010, 2013.

[18] Z. Li, J. Chen, Y. Zi, J. Pan, L. Chen, and Y. Y. Zi, "Independence-oriented VMD to identify fault feature for wheel set bearing fault diagnosis of highspeed locomotive," *Mechanical Systems and Signal Processing*, vol. 85, pp. 512–529, 2017.

[19] K. Dragomiretskiy and D. Zosso, "Variational Variational Mode Decompositionode decomposition," *IEEE Transactions on Signal Processing*, vol. 62, no. 3, pp. 531–544, 2014.

[20] J. Ding, L. Huang, D. Xiao, and X. Li, "GMPSO-VMD GMPSO-VMD Algorithm and Its Application to Rolling Bearing Fault Feature Extractionlgorithm and its application to rolling bearing Fault Feature extraction," *Sensors*, vol. 20, no. 7, p. 1946, 2020.

[21] X. Jiang, J. Wang, C. Shen et al., "An adaptive and efficient variational mode decomposition and its application for bearing fault diagnosis," *Structural Health Monitoring*, vol. 20, no. 5, pp. 2708–2725, 2021.

[22] X. Jiang, Q. Song, H. Wang et al., "Central frequency mode decomposition and its applications to the fault diagnosis of rotating machines," *Mechanism and Machine Theory*, vol. 174, Article ID 104919, 2022.

[23] Q. Song, X. Jiang, G. Du et al., "Smart multichannel mode extraction for enhanced bearing fault diagnosis," *Mechanical Systems and Signal Processing*, vol. 189, no. 189, Article ID 110107, 2023.

[24] Y. Miao, B. Zhang, C. Li, J. Lin, D. Zhang, and H. Li, "Feature Feature Mode Decomposition: New Decomposition Theory for Rotating Machinery Fault Diagnosisode decomposition:

new decomposition theory for rotating machinery fault diagnosis," *IEEE Transactions on Industrial Electronics*, vol. 70, no. 2, pp. 1949–1960, 2023.

[25] X. Yan, M. Jia, A. Yan, and P. Jia, "Bearing fault diagnosis via a parameter-optimized feature mode decomposition," *Measurement*, vol. 203, Article ID 112016, 2022.

[26] J. Y. Liu and B. L. Zhu, "The application of particle swarm optimization algorithm in the extremum optimization of nonlinear function," in *Proceedings of the IEEE 12th International Conference on Computer and Information Technology*, pp. 286–289, Ruzomberok, Slovakia, September 2012.

[27] H. Zheng, Y. Zhang, J. Liu et al., "A novel model based on wavelet LS-SVM integrated improved PSO algorithm for forecasting of dissolved gas contents in power transformers," *Electric Power Systems Research*, vol. 155, pp. 196–205, 2018.

[28] S. Mirjalili, A. Lewis, and A. Lewis, "The whale optimization algorithm," *Advances in Engineering Software*, vol. 95, pp. 51–67, 2016.

[29] J. Li, W. Chen, K. Han, and Q. Wang, "Fault Diagnosis of Rolling Bearing Based on GA-VMD and Improved WOA-LSSVMiagnosis of rolling bearing based on GA-VMD and improved WOA-LSSVM," *IEEE Access*, vol. 8, pp. 166753–166767, 2020.

[30] Y. Sun, X. Wang, Y. Chen et al., "A modified whale optimization algorithm for large-scale global optimization problems," *Expert Systems with Applications*, vol. 114, pp. 563–577, 2018.

[31] R. Deepa and R. Venkataraman, "Enhancing Whale Optimization Algorithm with Lévy Flight for coverage optimization in wireless sensor networks," *Computers & Electrical Engineering*, vol. 94, Article ID 107359, 2021.

[32] G. M. Viswanathan, V. Afanasyev, S. V. Buldyrev et al., "Lévy flight search patterns of wandering albatrosses," *Nature*, vol. 381, no. 6581, pp. 413–415, 1996.

[33] R. Gu, J. Chen, R. Hong et al., "Incipient fault diagnosis of rolling bearings based on adaptive variational mode decomposition and Teager energy operator," *Measurement*, vol. 149, Article ID 106941, 2020.

[34] W. He, Y. Zi, B. Chen, F. Wu, and Z. He, "Automatic fault feature extraction of mechanical anomaly on induction motor bearing using ensemble super-wavelet transform," *Mechanical Systems and Signal Processing*, vol. 54-55, pp. 457–480, 2015.

[35] W. A. Smith, R. B. Randall, A. Smith, and R. B. Randall, "Rolling element bearing diagnostics using the CaseWestern Reserve University data: Rolling element bearing diagnostics using the Case Western Reserve University data: A benchmark study benchmark study," *Mechanical Systems and Signal Processing*, vol. 64-65, pp. 100–131, 2015.